From leaf to soil: *n*-alkane signal preservation, despite degradation along an environmental gradient in the tropical Andes.

Milan L. Teunissen van Manen[1], Boris Jansen[1], Francisco Cuesta[2], Susana León-Yánez[3], William D. Gosling[1].

[1] Institute for Biodiversity and Ecosystem Dynamics (IBED), University of Amsterdam, Amsterdam, The Netherlands.

[2] Grupo de Investigación en Biodiversidad, Medio Ambiente y Salud (BIOMAS), Universidad de Las Américas (UDLA), Quito, Ecuador.

[3] Escuela de las Ciencias Biológicas, Pontificia Universidad de Católica de Ecuador (PUCE), Quito, Ecuador.

10   *Correspondence to*: M.L. Teunissen van Manen (M.L.TeunissenvanManen@uva.nl)

Abstract. Plant wax *n*-alkane biomarkers obtained from ancient soils and sediments have been used to reconstruct past environmental changes. However, the interpretation of these ancient n-alkane patterns relies primarily on our understanding of modern plant wax *n*-alkane patterns measured from leaves. Very little is known about how *n*-alkane patterns might be altered during the process of transfer from leaves into soil. Therefore our interpretations of the ancient *n*-alkane biomarker

15   signal could be confounded by an unobserved bias caused by degradation processes. Here we present the *n*-alkane patterns extracted from leaves, necromass and soil samples to clarify whether the *n*-alkane pattern, the *n*-alkane signal, and the local environmental information reflected in the *n*-alkane signal degrade, as the plant source material degrades in the tropical Andes. We find that the *n*-alkane patterns do degrade, but that the *n*-alkane patterns and signal remain similar across sample types. We find that the *n*-alkane patterns primarily reflect changes in longer *vs.* shorter *n*-alkanes, captured by the average

20   chain length (ACL) and the $C_{31}/(C_{29}+C_{31})$ ratio (ratio), regardless of sample type. Additionally, soil sample *n*-alkanes secondarily reflect changes in carbon preference index (CPI) whereas leaf and necromass *n*-alkanes do not. We find that in all sample types the primary observed *n*-alkane signals correlate significantly with the environment, temperature in particular, but that soil *n*-alkane correlations are muted compared to leaf *n*-alkanes. The secondary *n*-alkane signal (CPI) in soils also correlates significantly with the environmental signal, temperature in particular. Our results are an important step

25   towards better understanding the taphonomy of the *n*-alkane signal in the tropics, and suggest that environmental information is preserved in the *n*-alkane signal, despite the observed degradation.

1 Introduction

Making accurate reconstructions of past environments is important and urgent, as these can inform how modern environments could respond to current climatic and land use changes (Cronin, 2014). Interpretations of past environmental

30   change are commonly obtained from fossil pollen, charcoal, and molecular proxies extracted from sediments and soils (Smol

et al., 2001). To help improve these reconstructions of past environments and environmental change, new proxies such as plant wax *n*-alkanes are being developed (Eglinton and Eglinton, 2008; Jansen and Wiesenberg, 2017).

Plant wax *n*-alkanes (typically between C_{21}-C_{35}) are part of the protective outer wax layer of plants (Eglinton and Hamilton, 1967), and have been observed to reflect the local environmental conditions in which the plant is situated (for example, Feakins et al., 2016; Hoffmann et al., 2013; Teunissen van Manen et al., 2019). The *n*-alkanes produced by plants transfer to the soil and sedimentary records, where they are preserved and from which they can be extracted (Jansen and Wiesenberg, 2017). The retention of fossil *n*-alkanes in soils and sediments make *n*-alkanes a promising new proxy to help reconstruct environmental change (temperature and precipitation in particular) (Bush and McInerney, 2015; Hoffmann et al., 2013; Teunissen van Manen et al., 2019).

Multiple studies have already used plant wax *n*-alkane biomarkers to reconstruct past environmental change (Crausbay et al., 2014; Jansen et al., 2013). For example, Crausbay et al. (2014) reconstructed past drought frequency in a tropical montane cloud forest on the Haleakalā volcano (Maui, Hawaii, USA) using *n*-alkane patterns. Specifically, Crausbay et al. (2014) calibrated the fossil *n*-alkane record using the modern *n*-alkane signal of the *Metrosideros polymorpha* species, which has a pubescent and a glabrous variety. The modern pubescent and glabrous *n*-alkane calibration data were then used to reconstruct past abundance of pubescent *vs.* glabrous plant varieties and, from this infer relatively wet and dry conditions (Crausbay et al., 2014). In the Crausbay et al. (2014) study, and all other studies using *n*-alkanes biomarkers, the inferred past environmental changes from the ancient *n*-alkane record are reliant on what is known about modern plant wax *n*-alkanes and how they reflect the environment from which they were sampled. However, most of the studies on environmental controls of plant wax *n*-alkanes have been done on leaf material, often fresh from the tree. Very little is known about the complex pathway that *n*-alkanes undergo during the process of transfer from fresh leaf into soils and sediments. Our current understanding of the taphonomy of *n*-alkane patterns is based on the few studies done on necromass and soils (Bush and McInerney, 2015; Howard et al., 2018; Tipple and Pagani, 2013; Wu et al., 2019).

As the source (plant) material degrades, it is poorly understood whether and how the *n*-alkane patterns (the relative distributions of *n*-alkanes), the *n*-alkane signal (the dominant changes found in the *n*-alkane patterns) and the *n*-alkane environmental signal (how the *n*-alkane signal reflects the local environment) also degrade. This lack of knowledge on the taphonomy of the *n*-alkane signal means that our interpretations of the ancient *n*-alkane biomarker signal could be confounded by an unobserved bias caused by degradation processes (Wu et al., 2019). This could potentially lead to erroneous or biased inferences of past environmental change based on the *n*-alkane biomarker signal. Therefore, expanding our knowledge on the taphonomy of the *n*-alkane signal is key to reliably deploy plant wax *n*-alkane biomarkers to reconstruct past environmental change (Wu et al., 2019).

65   The study aim is to expand the knowledge on the taphonomy of the plant wax *n*-alkane signal by comparing the *n*-alkane patterns extracted from leaves, necromass and soils, sampled along an attitudinally driven environmental gradient in the tropical Andes (Ecuador). By choosing this particular gradient for our study we can build on the body of knowledge available on the transect (Pinto et al., 2018) and simultaneously elaborate on the *n*-alkane work previously done by us (Teunissen van Manen et al., 2019). Specifically, in this study we address: (1) whether the *n*-alkane pattern and signal

70   degrade as the source material degrades (i.e. are the *n*-alkane patterns found in leaves, necromass and soils similar?), and (2) whether the *n*-alkane signal preserves the environmental information observed in leaves as the source material degrades (i.e. do the *n*-alkane patterns found in leaves, necromass and soils reflect the environment similarly?). We will discuss our findings in light of the applicability and interpretation of the *n*-alkane biomarker records as a proxy for local environmental change in the past.

75   **2 Materials and methods**

2.1 Study site and sampling

This study utilized the Pichincha long-term forest development and carbon monitoring transect, situated on the north western flank of the Ecuadorian Andes (Fig. 1). The sampled transect was established in 2015 by the research non-profit organization Consorcio para el Desarrollo Sostenible de la Ecorregión Andina (CONDESAN) (http://condesan-ecoandes.org/), who

80   catalogued the tree community composition and recorded environmental data at each permanent plot (hereafter 'plot') (Pinto et al., 2018; Pinto and Cuesta, 2019).

The extensive elevation gradient captured by the transect, between 632 and 3507 m a.s.l. (above sea level), induces multiple environmental gradients, among which temperature, humidity and precipitation gradients. Mean annual temperature and

85   mean annual relative air humidity ('temperature' and 'humidity' hereafter) were calculated based on hourly data collected at each plot between 2016-2018 (see Teunissen van Manen et al. (2019) for more details). We obtained the plot annual precipitation (hereafter 'precipitation') from the CHELSA dataset at 30S resolution (1km) (Karger et al., 2017). In total, the transect temperature gradient spans 7.2- 21.6 °C, the humidity gradient spans 96.1 - 99.8% and the precipitation gradient spans 1580 - 2448 mm.

90

All samples were collected from the Pichincha transect (Table 1). Each plot (60x60 m) was subdivided in 9 subplots of 20x20m. The leaf samples were collected and analysed in a previous study (Teunissen van Manen et al., 2019). For that study we targeted two widely distributed genera along the transect, the *Miconia* and *Guarea* genera (see Teunissen van Manen et al. (2019) for the genus distributions along transect) (Pinto et al., 2018). From each individual we took one sample,

95   which consisted of 20-25 leaf(lets) taken from the canopy. In total we collected 87 leaf samples from 14 plots (Table 1). For this study these samples were supplemented with new necromass and soil samples.

Necromass samples were collected from the three plots were necromass traps were available(Pinto and Cuesta, 2019). At each of those plots, five subplots had necromass traps installed. From each necromass trap we took one sample, which consisted of five randomly selected leaves. In total we collected 15necromass samples from three plots (Table 1).

100

Soil samples were collected at every plot. At each plot we selected the centre subplot and two randomly selected subplots from which to sample soils. From each subplot we took one sample, which consisted of 10 "pinches" of surface soil randomly taken across the subplot (we removed the necromass layer to access the surface soil where necessary). We unintentionally sampled one extra subplot at one of the plots (MALO_01, Table 1). In total we collected 43 soil samples

105   from 14 plots (Table 1).

All samples were collected with gloved (latex) hands and wrapped in aluminium foil in the field, making sure no contact was made with the skin to avoid lipid contamination. Samples were bagged and placed in a cold storage (5 $^{\circ}$C) until further analysis at the University of Amsterdam.

110   **2.2 *n*-Alkane extraction and quantification**

Leaf data was previously extracted and quantified by Teunissen van Manen et al. (2019). Necromass and soil samples were analysed following the same protocol. Necromass and soil samples were freeze dried and milled to powder. Soil samples were analysed for carbon content in an Elemental Vario El Cube. Necromass samples were assumed to contain c. 50% carbon. Depending on carbon content, between 0.1-0.5 g of sample was extracted using a Dionex 200 accelerated solvent

115   extractor (ASE). With every extraction set we ran a blank sample that was treated as if it were a regular sample. The internal standard consisted of a mixture of 5α-androstane, androstanol, and erucic acid (0.33 µg/µL per compound) 40 µl of internal standard was added to each sample prior to extraction. The extracted solution was dried under steady stream of N_2 to remove the solvent, and re-dissolved in 1mL hexane.

120   The *n*-alkane fraction was obtained by eluting a 10 mL solid phase column (approximately 1.5 g of silica gel, 5% deactivated H_2O, previously conditioned with acetone, dichloromethane and hexane) with approximately 7mL hexane in multiple steps. The resulting *n*-alkane fraction was again dried under a stream of N_2, re-dissolved into 1 mL hexane, and finally analysed using gas chromatography-mass spectrometry (GC-MS) with quadruplet detection in full scan mode. The GC-MS protocol was as follows: the sample was injected in a DB5 column (30 m) under constant flow of gas helium at 0.8 mL/min. Start at

125   50 °C (hold 2 min); first ramp at 60 °C/min to 80 °C (hold 2 min); second ramp at 20 °C/min to 130 °C (no hold); third ramp at 4 °C/min to 350 °C (hold 10 min).

Identification and quantification of *n*-alkanes was done by comparing measurements with a known mixture of *n*-alkanes in the range C_{25}-C_{33}, and the internal standard employing the Thermo Xcalibur® software. Limit of detection (LOD) was set at

130   3x the base level, any concentration below was set to "not found". The resulting *n*-alkane dataset was standardized to sample weight (grams of dry sample used for extraction). To estimate measurement variability, replicate measurements were done on four necromass and 26 soil samples. Fourteen replicate measurements of the leaf samples were previously measured and reported on in detail Teunissen van Manen et al. (2019).

    Not all samples retrieved from the field were analysed successfully, in three samples we measured only sporadic *n*-alkane

135   peaks (Table 1). In total 86 leaf samples, 13 necromass samples, and 51 soil samples were considered robust data and were used for further data analysis (Table 1).

2.3 Data analysis

2.3.1 Standardization

    The measured *n*-alkanes ranges differed between leaf, necromass and soil samples (C_{23}-C_{33}, C_{21}-C_{33}, and C_{15}-C_{33},

140   respectively). In order to compare the datasets, we standardized the measured *n*-alkane range to the shortest range, between C_{23}-C_{33}. We found this had no visible effect on the results, likely because the chain lengths below C_{23} contained only a small proportion of the total *n*-alkane fraction, which has also been observed before (Ardenghi et al., 2017). The *n*-alkane concentrations of replicate samples were averaged before continuing data analysis.

2.3.2 Multivariate analysis of *n*-alkane patterns

145   We standardized the *n*-alkane data to total *n*-alkane concentration (CONw) to obtain the relative abundance of each chain length (%). Where CONw is the sum of all *n*-alkane concentrations standardized to dry sample weight (ng/g of dry sample). We used these data as input for non-metric multidimensional scaling (nMDS) analysis on each sample type and on all sample types combined (four analyses in total). The aim was to identify the major *n*-alkane patterns defining each sample type and to also compare the sample types. We performed the nMDS using the metaMDS function, from the 'vegan'

150   package (Oksanen et al., 2018) in RStudio (R Core Team, 2017), with Euclidean distance matrix and disabling the default data transformation intended for species community data. We fitted the environmental variables (temperature, humidity and precipitation) to the nMDS in order to help identify environmental correlations with the *n*-alkane patterns. We also used the standardized *n*-alkane data to produce the transect average *n*-alkane distributions (and standard deviation) per sample type.

2.3.3 *n*-Alkane metrics

155   We calculated three common metrics used in *n*-alkane biomarker studies, namely the ACL, the normalized ratio between C_{31}/C_{29}, and the CPI (hereafter, 'the metrics'). The ACL was calculated following the Bush & McInerney (2013) Eq. (1):

$$ACL_{23-33} = \frac{\Sigma(C_n \times n)}{\Sigma C_n} \qquad\qquad\qquad (1)$$

Where C_n is the concentration of n-alkane per gram of dried sample and n is the number of carbon atoms of an n-alkane

160   between C_{23} and C_{33}. The ratio between C_{31} and C_{29} $_n$-alkanes was calculated following the Bush & McInerney (2013) Eq. (2):

$$\text{ratio} = \frac{C_{31}}{C_{31}+C_{29}} \qquad\qquad (2)$$

165   The n-alkane carbon preference index (CPI) values were calculated following the Marzi et al. (1993) Eq. (3):

$$CPI_{23-33} = \frac{[\,\Sigma_{odd}(C_{23-31}) + \Sigma_{odd}(C_{25-31})\,]}{2(\Sigma_{even}C_{24-32})} \qquad\qquad (3)$$

Where Σ_{odd} is the sum of all concentrations of odd chain n-alkanes between and including the indicated n-alkane chain

170   length ranges, and Σ_{even} is the sum of all concentrations of even chain n-alkanes between C_{24}-C_{32}.

2.3.4 Environmental correlations

We generated a correlation matrix with the environmental variables (altitude, temperature, humidity and precipitation), the metrics and the nMDS axes per sample type, to identify: (1) whether the n-alkane metrics captured dominant changes in the n-alkane patterns (the nMDS), and (2) whether the n-alkane signal (the metrics and the nMDS axes) and the environmental

175   variables correlate. The Pearson's linear correlation matrices were calculated using the 'corrplot' (Wei and Simko, 2017) and 'Hmisc' (Harrell and Dupont, 2019) packages in RStudio (R Core Team, 2017). We adopted a significance threshold value of $p < 0.01$ because the bulk of our analysis are correlations; as is convention (Teunissen van Manen et al., 2019; Tipple and Pagani, 2013). All data analysis was done in RStudio using the base functions (R Core Team, 2017) and the 'tidyverse' packages functions (Wickham, 2017).

180   **3 Results**

The replicate measurements showed that absolute concentration of n-alkanes varied more than 10% from the mean (CV%) in the majority of the replicate samples, with CV% values ranging from 11.5% to 48% (Table A1). The high variability in absolute concentration in the replicate samples could be due to sample heterogeneity despite the elaborate sample homogenization process prior to extraction. Despite the high variability in absolute concentrations, the relative distributions

185   of the replicate samples showed almost no variability (Fig. B1), giving us confidence that the metrics and relative abundances presented are robust.

The transect average *n*-alkane patterns of each sample type reflected a typical higher terrestrial plant distribution, with a clear odd-over-even distribution between the ranges of C_{23} and C_{33} (Fig. 2, Fig. B1). The three sample types had similar average distributions of the chain lengths (Fig. 2). Specifically, they shared dominant C_{29} and C_{31} chain lengths, with an average contribution of ±30-40% of CONw each (Fig. 2). Although the transect average proportion of C_{27} differed somewhat per sample type, the variability across the transect is very high, in necromass in particular (Fig. 2).

3.1 Identification of the dominant changes in the *n*-alkane patterns

3.1.1 Description of the patterns

The nMDS analyses exposed the variability in the *n*-alkane patterns of each sample type (Fig. 3 a,b,c) and how the sample type patterns compare (Fig. 3d). Notably, the first axis of all the nMDS plots were driven by a shift in relative abundance from shorter *n*-alkanes ($\leq C_{29}$, lower end of the axis) to longer *n*-alkanes ($>C_{29}$, higher end of the axis) (Fig. 3a,b,c,d).

It is less clear what variability in the *n*-alkane patterns drove the samples to spread along the second nMDS axis. However, some even numbered chain lengths were placed on the higher end of the second axis of the leaf and soil nMDS plots (Fig. 3a,c). This indicates that the samples on the higher end of the second axis of the leaf and soil nMDS plots had relatively higher abundances of those even numbered chain lengths (Fig. 3a,c).

The nMDS analysis of all sample types together shows that the different sample types did not cluster or separate from each other, although the soil data did scatter less than the leaf and necromass data (Fig. 3d). The lack of separation and significant clustering indicates that the sample type patterns were not significantly different or distinguishable from each other.

3.1.2 Identification of the signal in terms of metrics

For all sample types, correlations between the first nMDS axis and the ACL and ratio metrics were significant (Fig. 4, Table 2), which indicates that the change in patterns captured by the first nMDS axis of all sample types are explained by shifts in ACL and ratio (Fig. 4). It should be noted that these two metrics were highly correlated across sample types (leaf: r = 0.9, p-value <0.001; necromass: r = 0.8, p-value <0.001; soil: r = 0.9, p-value <0.001) (Fig. 4, Table 2). The high correlation between ACL and ratio indicates that both metrics captured shifts in relative abundances of shorter *vs.* longer *n*-alkane chain lengths, and accurately described the dominant shifts in the *n*-alkane patterns of all sample types in this study. Notably, the CPI metric did not correlate with the first nMDS axis of any sample type (leaf: r = 0.1, p-value = 0.389; necromass: r = -0.2, p-value = 0.426; soil: r = -0.2, p-value = 0.291) (Fig. 4, Table 2).

Correlation between the second nMDS axis and the metrics differed per sample type. The second axis of the leaf data nMDS correlated with the ACL and CPI metrics (r = -0.4, p-value < 0.001 and r = -0.3, p-value = 0.005, respectively) (Fig. 4a, Table 2). However, these correlations were non-significant when the samples separating from the main clusters on the top

left of the leaf nMDS plot were removed from the analysis (Fig. 3a, Fig. C1). These four samples represent a single species

220   sampled at a one plot at high altitude (Teunissen van Manen et al., 2019). Therefore, the changes in the leaf *n*-alkane pattern

captured by the second nMDS axis could not be identified by commonly used metrics.

The second axis of the necromass data nMDS did not significantly correlate with any of the metrics (Fig. 4b, Table 2). The

changes in the necromass *n*-alkane pattern captured by the second nMDS axis could not be identified by commonly used

225   metrics.

The second axis of the soil data nMDS correlated with the CPI metric (r = -0.5, p-value < 0.001), which indicates that the

change in patterns captured by the second nMDS axis of the soil data was partially reflected by shifts in CPI (Fig 4c, Table

2). However, the correlation was not complete, therefore some changes in the soil *n*-alkane patterns (as captured by the

230   second nMDS axis) remained un-attributable to commonly used metrics.

3.2 Environmental signal of the *n*-alkane patterns

The environmental variables (altitude, temperature, humidity and precipitation) highly co-correlated (Fig 4a,b,c, Table 2), in

particular altitude and temperature were exact opposites (r = -1, p-value <0.00, regardless of sample type). This is to be

expected as we sampled along a single altitudinal gradient. In order to avoid repetition, we will focus the remainder of the

235   results and the discussion on the temperature, humidity and precipitation variables only.

The dominant changes in the leaf *n*-alkane patterns, identified as changes in the ACL and ratio metrics, correlated positively

with the environmental variables (Fig. 3a, Fig. 4a, Fig. 5, Table 2). Although CPI did not significantly correlate with any of

the pattern shifts captured by the nMDS (after removing the one species separating from the rest) (Fig. 3a), the leaf data CPI

240   did significantly correlate with humidity (r = -0.4, p-value <0.001) (Fig. 4a, Fig. 5, Table 2).

The dominant changes in the necromass *n*-alkane patterns, identified as changes in the ACL and ratio metrics, did not show

any significant correlations with the environmental variables (Fig. 3b, Fig. 4b, Fig. 5, Table 2). This was most likely due to

the limited number of samples that were collected along the transect (Table 1).

245

The dominant changes in the soil *n*-alkane patterns, identified as changes in ACL, ratio and CPI, correlated with temperature

in particular (r = 0.6, p-value <0.001, r = 0.5, p-value <0.001 and r = -0.4, p-value <0.001, respectively) (Fig. 3c, Fig. 4b,

Fig. 5, Table 2). Additionally, soil ACL and CPI also correlated with precipitation (r = 0.4, p-value = 0.001 and r = -0.4, p-

value = 0.005) (Fig. 4c, Fig. 5, Table 2).

4 Discussion

4.1 *n*-Alkane patterns and what they signal at different stages of source degradation

4.1.1 Do the *n*-alkane patterns degrade significantly?

The *n*-alkane patterns (i.e. the relative chain length distribution) of all sample types reflected those typical of higher terrestrial plants (Eglinton and Hamilton, 1967), suggesting that *n*-alkane patterns do not degrade considerably (Fig. 2). This is corroborated by the nMDS results, which indicate the *n*-alkane patterns from all stages of degradation are indistinguishable from each other, although soil *n*-alkane patterns did show less variance than necromass and leaves *n*-alkane patterns (Fig. 3d). These results fall in line with the results presented in the few studies that have compared leaf and soil *n*-alkanes, who also find similar distributions of leaf *n*-alkanes and soil *n*-alkanes (Howard et al., 2018; Tipple and Pagani, 2013). Large variance in leaf *n*-alkane patterns has been observed before (Bush and McInerney, 2013; Carr et al., 2014), but was never directly compared to necromass or soil *n*-alkane variability. Our results give a first indication that necromass *n*-alkanes patterns can vary to the same large extent that leaf *n*-alkane patterns do, whereas soil *n*-alkanes patterns exhibit a more muted variance, likely owing to the spatiotemporal mixing of the input (Howard et al., 2018; Wu et al., 2019). These findings suggest that the *n*-alkane pattern does not degrade considerably as the plant source degrades, but that some information is lost once reworked into soils.

4.1.2 Does the signal reflected in the *n*-alkane patterns degrade?

Our results indicate that the *n*-alkane patterns extracted predominantly vary in the relative abundance of longer *vs.* shorter *n*-alkanes, regardless of stage of degradation (Fig. 3a,b,c,d), suggesting that the *n*-alkane signal does not drastically degrade as the plant source material degrades. In our study, the ACL and ratio metrics reflected the *n*-alkane signal, independent of sample type.

In addition to the predominant *n*-alkane signal across sample types, our results indicate that soil *n*-alkane patterns vary in the relative abundance of odd *vs.* even *n*-alkanes (Fig. 3c). This secondary signal in soil *n*-alkanes is reflected in the CPI metric (Fig. 4c). *n*-Alkane patterns from leaf and necromass samples did not reflect an odd *vs.* even signal in our study (once we account for the four samples (one species) that separate from the bulk of the leaf data) (Fig. 3a,b, Fig. 4a,b).

CPI is a metric specifically developed to capture changes in odd-over-even predominance, and is thought to reflect degradation (Marzi et al., 1993). Our results show that only the soil *n*-alkane signal reflects changes in CPI, which suggests that the processes leading to changes in CPI are related to soil processes. Potentially, such a process could be the de-novo genesis of *n*-alkanes without an odd-over-even predominance as a result of microbial alteration (Brittingham et al., 2017; Jansen and Wiesenberg, 2017; Rao et al., 2009; Wu et al., 2019), although this should be studied more extensively. Notably, the CPI does not correlate with the ACL and ratio metrics (Fig. 4c), indicating that the dominant signal (changes in longer *vs.*

shorter *n*-alkanes) is not affected by the secondary signal (changes in odd *vs.* even *n*-alkanes) in soils. This confirms previous indications that soil degradation processes do not drastically alter the ACL, but instead alter the odd-over even predominance (i.e. CPI) (Howard et al., 2018).

285 **4.2 Preservation of the environmental information in *n*-alkane signals across sample types**

We find that the systematic variance in longer *vs.* shorter *n*-alkanes in leaf and soil samples, also reflected in the ACL and ratio metrics, positively correlates with precipitation and, in particular, temperature (Fig. 4a,c, Fig. 5). These findings fall in line with previous observations in leaf and soil data (Bush and McInerney, 2015; Tipple and Pagani, 2013). However, our results also show that the strength of the observed correlations diminishes slightly as the source material degrades (Fig. 4a,c,

290 Fig. 5). This is also reflected in the lower variance observed in the soil ACL and ratio metrics (nMDS axis 1, Fig. 3d). These results suggest that the *n*-alkane signal along the altitudinal gradient reflects local environmental conditions, temperature in particular, but are somewhat muted once the source material degrades (Fig. 4a,c, Fig. 5). The results from previous work that report leaf and soil *n*-alkane ACL values along a (latitudinal) temperature gradient are mixed. Bush and McInerney (2015) found a stronger correlation between soil ACL and temperature than plant ACL and temperature in the USA. Also in the

295 USA, Tipple and Pagani (2013) found that the soil and plant ACL correlation with temperature were in the same order of magnitude. However, the difference between our results and previous work can be explained by the differences in the leaf data used in these studies, where one study focusses on two particular species and the other study sampled both woody and herbaceous plants (Bush and McInerney, 2015; Tipple and Pagani, 2013). A third study reporting on leaf and soil ACL data from South Africa, found no relation to temperature or precipitation but they noted this was due to the short environmental

300 gradient sampled (Carr et al., 2014). It should be noted that the muted correlations in soil *n*-alkanes in our study are likely not a result of (preferential) degradation of the *n*-alkane signal, as ACL and CPI are uncorrelated (Fig. 4c). Alternatively, the muted soil ACL and temperature correlation observed in our study could be due to soil *n*-alkanes reflecting an average of a larger spatial/temporal scale than that reflected in leaves (Howard et al., 2018; Wu et al., 2019). The overall reduction of the range of variability in the soil *n*-alkane patterns (compared to leaf *n*-alkane patterns) supports this idea (Fig. 3d), but further

305 research is needed.

The secondary signal in soil *n*-alkane patterns, characterized as changes in odd *vs.* even *n*-alkanes and reflected in the CPI metrics, inversely correlates with temperature and precipitation (Fig. 4c). The inverse correlation between temperature and soil CPI has been observed before in soils and has been hypothesized to be due to increased microbial degradation of *n*-

310 alkanes under favourable (warm and wet) conditions, independent of local standing vegetation (Luo et al., 2012; Rao et al., 2009). Along an altitudinal transect in Peru similar to our study, lower CPI values at lower elevations (warmer) have also been observed in soils and suspended river sediments (Feakins et al., 2018; Wu et al., 2019). Contrastingly, Bush and McInerney (2015) do not find a clear correlation between soil CPI and environment. However, the Bush and McInerney

(2015) study was done along a latitudinal gradient in the USA so it is possible that the relationship is not perceived in all
315   ecosystems, and instead particular to the tropical settings of this study.

We do not find that leaf *n*-alkane patterns are characterized by changes in CPI once the single species effect is accounted for
(Fig. 3a, Fig. 4a, Fig. C1), suggesting that CPI is not an important descriptor of leaf *n*-alkane patterns. Despite this, the CPI
metric does negatively correlate with humidity (Fig. 5). The relationship between leaf *n*-alkane CPI values and the
320   environment is understudied, and no literature is available on the relationship between humidity and leaf CPI in particular.
However, the available previous findings report no systematic variation of leaf CPI values with other environmental
gradients (Bush and McInerney, 2015; Carr et al., 2014; Feakins et al., 2016; Wang et al., 2018), supporting the idea that CPI
is a weak descriptor of leaf *n*-alkane patterns.

4.3 Implications for *n*-alkanes as a proxy for past environmental change

325   While our study comprised a single transect along the Ecuadorian Andes, our results fall in line with previous findings from
other studies, both in similar settings and in other ecosystems and climatic regions. While such other studies did not
explicitly focus on degradation of *n*-alkane patterns from leaves through necromass to soil, the data they do report is
generally consistent with our findings.

330   Together with previous findings (Bush and McInerney, 2015; Teunissen van Manen et al., 2019; Tipple and Pagani, 2013),
our results suggest that *n*-alkane patterns vary predominantly in the relative abundances of longer *vs.* shorter *n*-alkanes,
which consistently reflected in the ACL and ratio metrics in our study, regardless of degradation level. If *n*-alkane
biomarkers in sedimentary records also reflect this direction of variance, it would suggest that the *n*-alkane patterns are
comparable to leaf and soil samples, and thus that interpreting the *n*-alkane biomarker record based on knowledge from
335   modern *n*-alkane patterns is valid. However, the large differences in variability between the sample types should be noted,
leaf *n*-alkanes being highly variable and soil *n*-alkanes less. The decreased variability of soil *n*-alkane patterns has been
noted before and has been attributed to degradation of the *n*-alkane signal in soils and the averaging qualities of soil samples
(Bush and McInerney, 2015; Howard et al., 2018; Wu et al., 2019). Therefore, when comparing ancient *n*-alkane records to
modern leaf data the larger variability of leaf *n*-alkane patterns and responses should be kept in mind, as sedimentary *n*-
340   alkane records are unlikely to reflect the same range of responses. Additionally, results from Wu et al (2019) suggest that
soil *n*-alkanes are a quantitatively important source of sedimentary *n*-alkane records. Therefore, although our results suggest
that the *n*-alkane signal remains comparable, basing *n*-alkane record interpretations of modern leaf data could lead to over- or
underestimation of the inferred environmental change. One way to overcome this, is to interpret the ancient *n*-alkane record
based on calibrations of modern soil *n*-alkanes rather than on modern plant *n*-alkanes.

345

The *n*-alkane signals in leaf and soils reflected environmental conditions, but the correlations between the metrics (ACL and ratio) and the environment decreased as the source material degraded (Fig. 4, Fig. 5). This suggests that in sedimentary records, the changes in the *n*-alkane biomarker signal likely underestimate past environmental change. However, there is insufficient knowledge on the extent to which the sedimentary *n*-alkane metrics underestimate environmental conditions at the time of deposition, and on post-sedimentary alteration of the *n*-alkane signal in general, to confidently infer the magnitude of environmental change based on the *n*-alkane record alone.

Corrections to counter the ancient *n*-alkane signal potential underestimation of inferred changes have been proposed, specifically using CPI as an indicator of *n*-alkane signal degradation (Buggle et al., 2010). Although there is evidence for convergence of CPI with the *n*-alkane ratios in sediments (Buggle et al., 2010), evidence in soils does not confirm the need to correct the *n*-alkane signal (ACL, ratio) for degradation (CPI), as it seems that the ACL and ratio are not drastically altered due to soil degradation processes but instead mostly alter the CPI of the *n*-alkanes.

The value of CPI as a proxy has been up for discussion, as plant data varied largely and with no systematic variability with environmental conditions observable (Bush and McInerney, 2013; Carr et al., 2014; Feakins et al., 2016; Wang et al., 2018). However, this illustrates how knowledge from leaf *n*-alkane signals does not directly translate to the *n*-alkane biomarker record, as it overlooks soil processes which can imprint environmental information in the *n*-alkane signal (this study, Wu et al., 2019). In our study and in previous work, soil CPI has been observed to vary with temperature (Luo et al., 2012; Rao et al., 2009) suggesting that the *n*-alkane biomarker signal has a secondary way of reflecting environmental conditions due to soil processes, most likely microbial degradation of the *n*-alkane signal by altering the even-chain length in the *n*-alkane pattern. However, this signal is likely dependent of the study region, as studies conducted outside of tropical settings have not observed the correlation between soil CPI and environmental (warm/wet) conditions.

Taken together, our results and previous findings regarding the interpretation of the *n*-alkane signal in terms of ACL, ratio and CPI, suggest that ancient *n*-alkane signals likely carry environmental information similar to that observed in modern leaves, necromass and soils. However, the exact interpretation is difficult, as many (understudied) aspects such as regional climatic setting and post-depositional alteration of the *n*-alkane signal potentially affect what the ancient *n*-alkane record reflects.

5 Conclusion

We find that the *n*-alkane pattern degrades but that leaf, necromass and soil sample *n*-alkanes remain comparable. This suggests that interpreting past *n*-alkane biomarkers based on modern *n*-alkane patterns is possible. In our study, the *n*-alkane signal in leaf and soils reflects local environmental conditions, temperature in particular, but soil *n*-alkanes underestimate the local conditions. Finally, we observe that the soil *n*-alkane signal also reflects local temperature in the CPI metric, which

offers the opportunity for a temperature metric independent of ACL. However, our findings, taken together with previous work, suggests that many understudied processes affect the *n*-alkane signal as it degrades, which makes interpreting and

380 inferring environmental change from sedimentary *n*-alkane records difficult. Our results highlight the need for better understanding of the taphonomy of higher plant *n*-alkanes if the *n*-alkane proxy is to be fully understood.

Data availability

All data presented in this manuscript is available on Figshare: https://doi.org/10.21942/uva.10299068

385 **Appendices**

Appendix A

Table A1: Sample replicates table, denoting: the replicate sample field code (sample), replicate sample type (type), the replicate sample average *n*-alkane concentration in ng/g of dried sample (CONw), the associated standard deviation (SD), coefficient of variance (CV(%)) and the number of replications done (N).

SAMPLE	TYPE	CONw	±SD	CV(%)	N
1	necromass	269.34	62.24	23.1	3
12	necromass	342.74	40.04	11.7	3
14	necromass	788.67	244.28	31.0	3
7	necromass	444.65	39.16	8.8	3
BIOM 003	soil	227.71	32.84	14.4	2
BIOM 006	soil	138.49	7.38	5.3	3
BIOM 007	soil	167.98	28.26	16.8	6
BIOM 010	soil	322.17	5.83	1.8	3
BIOM 015	soil	251.93	65.95	26.2	2
BIOM 018	soil	48.64	12.66	26.0	6
BIOM 019	soil	37.01	1.55	4.2	2
BIOM 022	soil	90.00	13.01	14.5	6
BIOM 024	soil	127.41	2.69	2.1	2
BIOM 025	soil	66.42	16.21	24.4	2
BIOM 026	soil	136.65	24.95	18.3	3
BIOM 027	soil	114.12	2.19	1.9	2
BIOM 028	soil	237.27	32.63	13.8	3
BIOM 032	soil	129.86	5.60	4.3	3
BIOM 033	soil	166.04	30.86	18.6	2
BIOM 036	soil	196.50	94.24	48.0	2
BIOM 038	soil	57.83	13.13	22.7	3
BIOM 040	soil	1094.09	155.69	14.2	3
BIOM 046	soil	167.32	30.76	18.4	3
BIOM 049	soil	396.95	15.78	4.0	5
BIOM 050	soil	104.22	7.69	7.4	2
BIOM 051	soil	136.15	42.57	31.3	3
BIOM 053	soil	61.85	7.12	11.5	2
BIOM 056	soil	158.34	25.50	16.1	3
BIOM 057	soil	180.53	16.65	9.2	3
BIOM 058	soil	136.85	34.39	25.1	2

390

Appendix B

Figure B1: Sample fingerprints, relative abundances (%) of the *n*-alkane chain lengths per sample. Samples that were measured repeatedly show average relative abundance (%) and standard deviation from the average relative abundance (lines), also see

395 **Table A1. Graph titles reference to sample field codes and sample type, where numbers without prefix indicate necromass samples, the BIOM prefix indicates soil samples and the GK, MCL, MTH, MBR, MCO and MOC prefix indicate plant samples (1/6).**
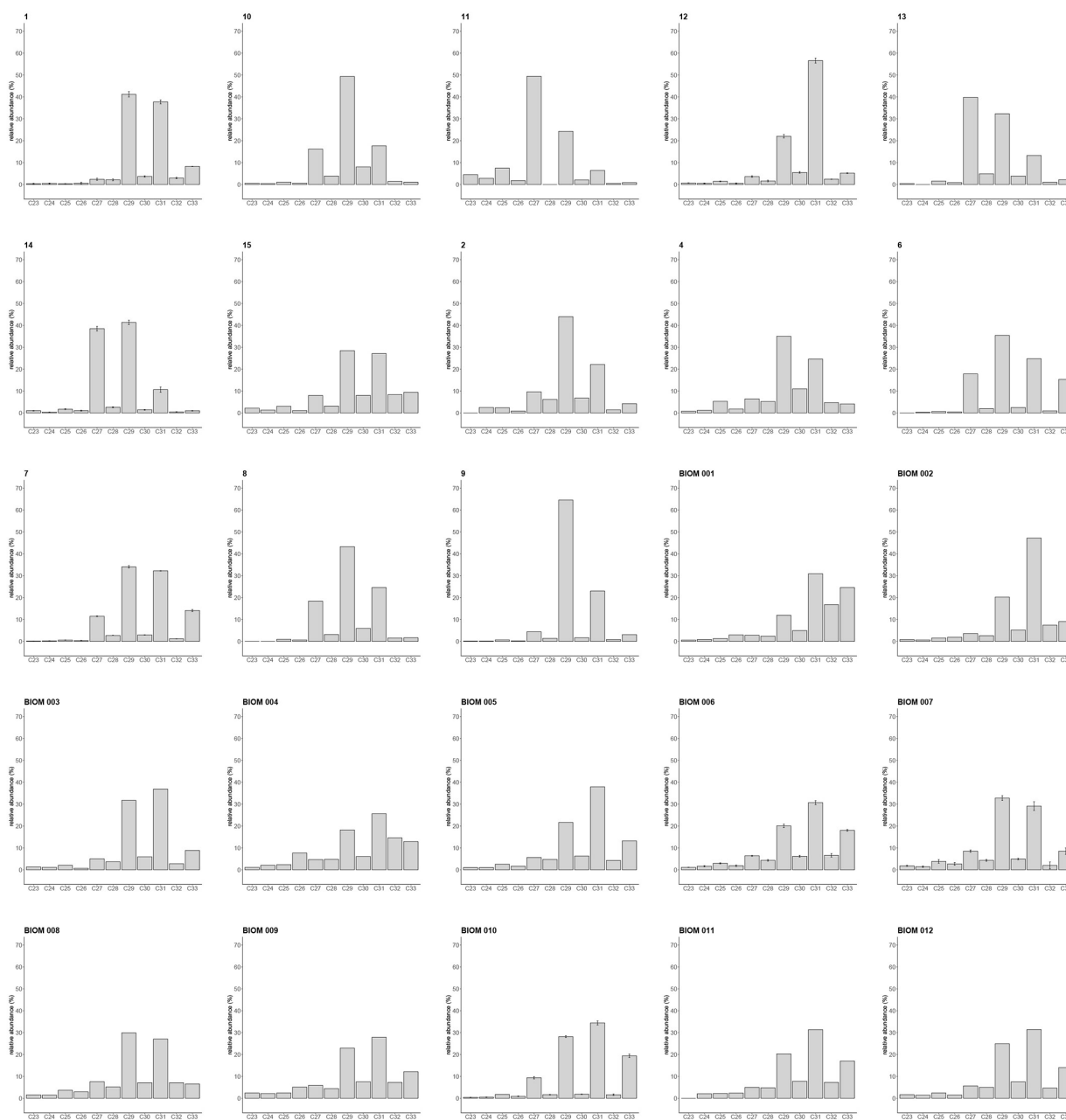
Figure B1 (continued, 2/6)

400
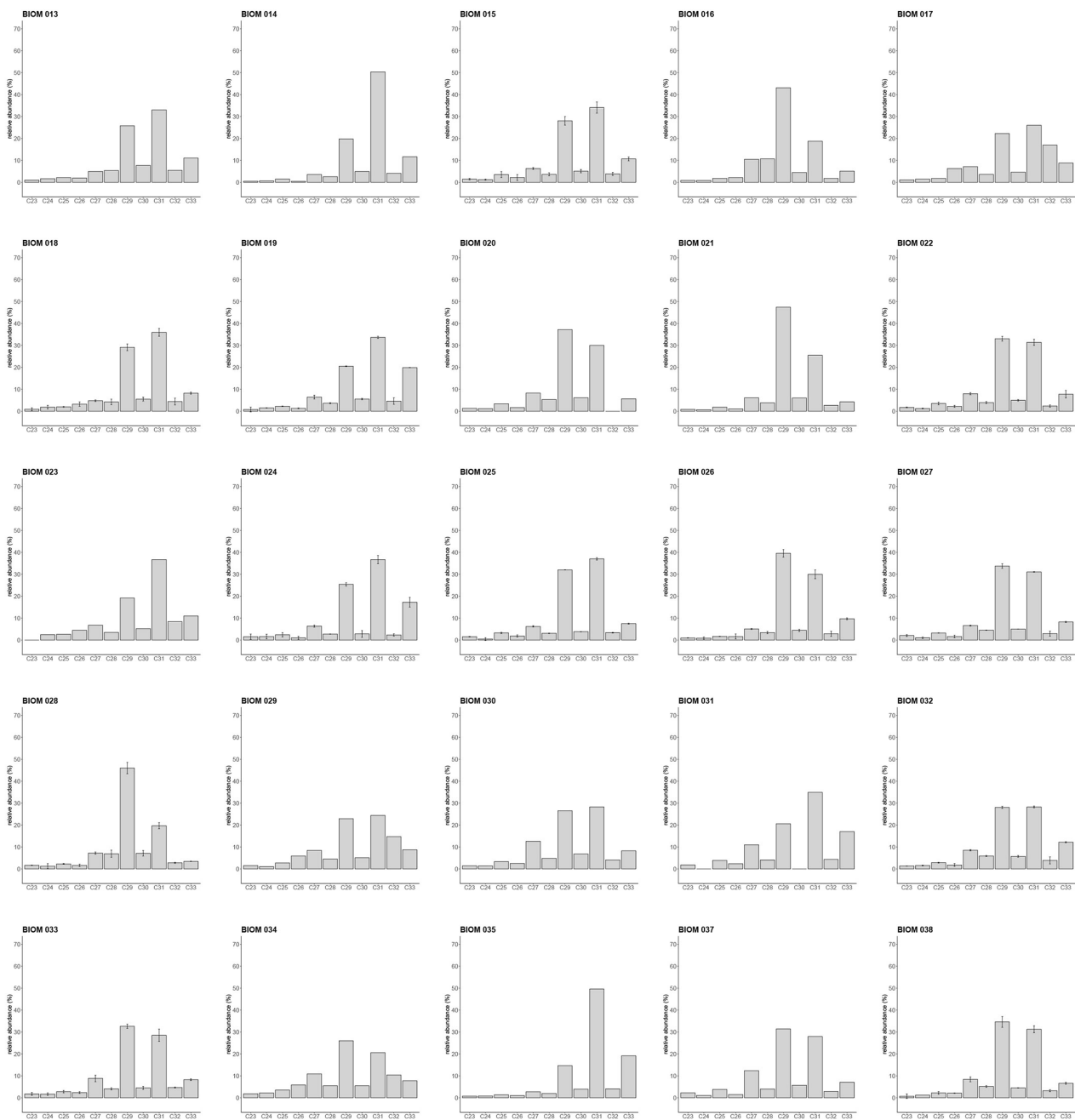
Figure B1 (continued, 3/6)
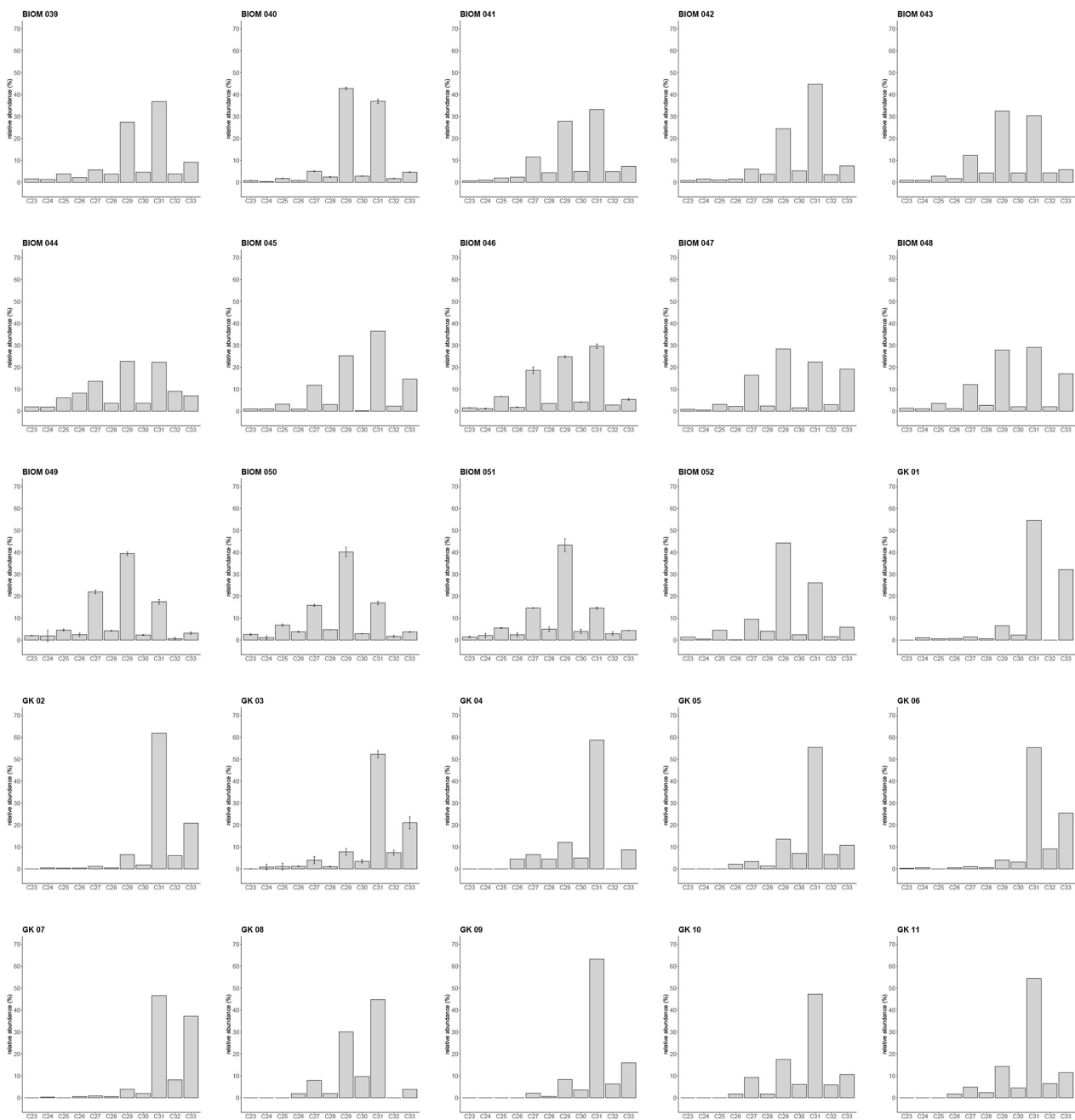
Figure B1 (continued, 4/6)

405
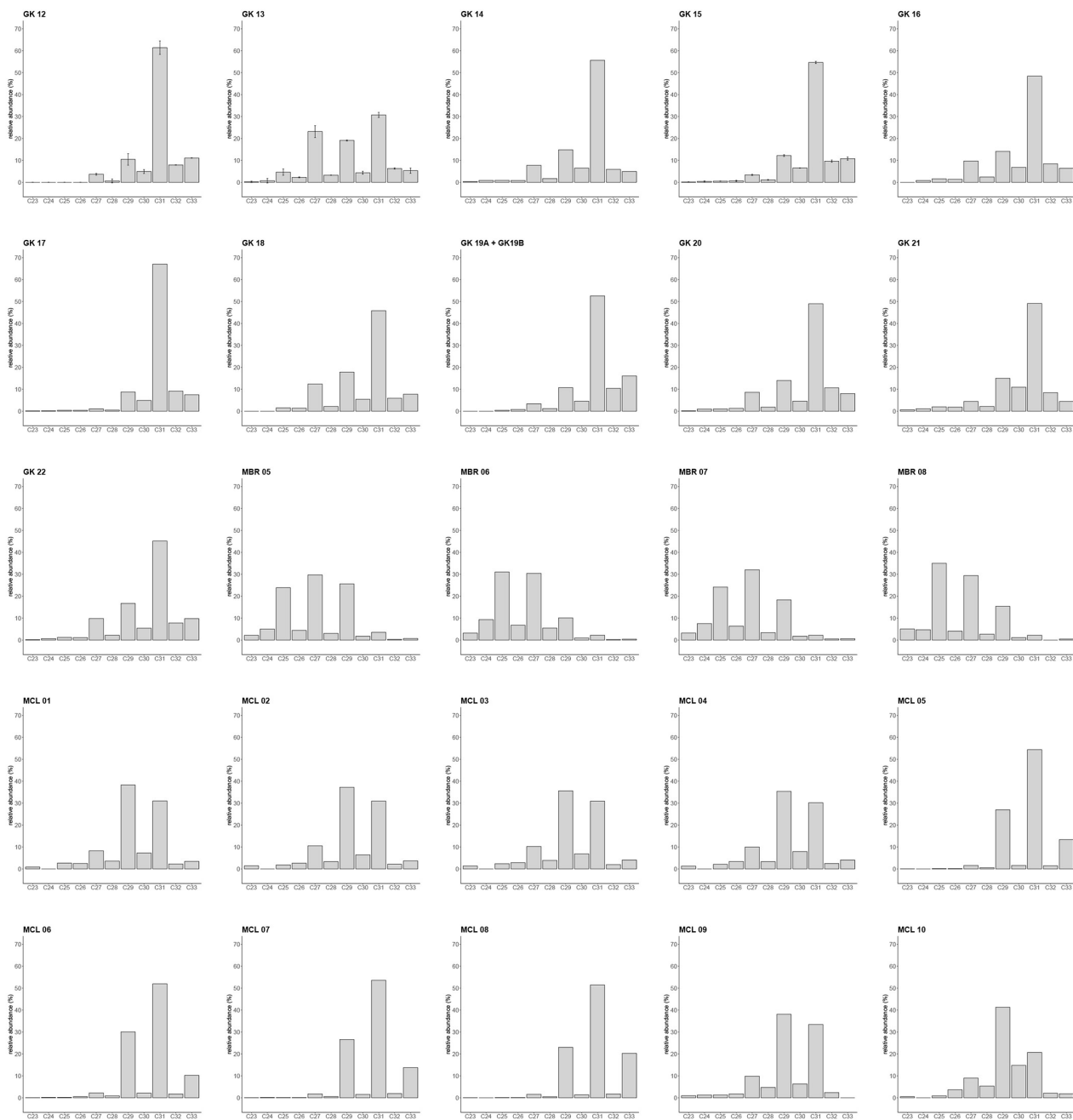
Figure B1 (continued, 5/6)
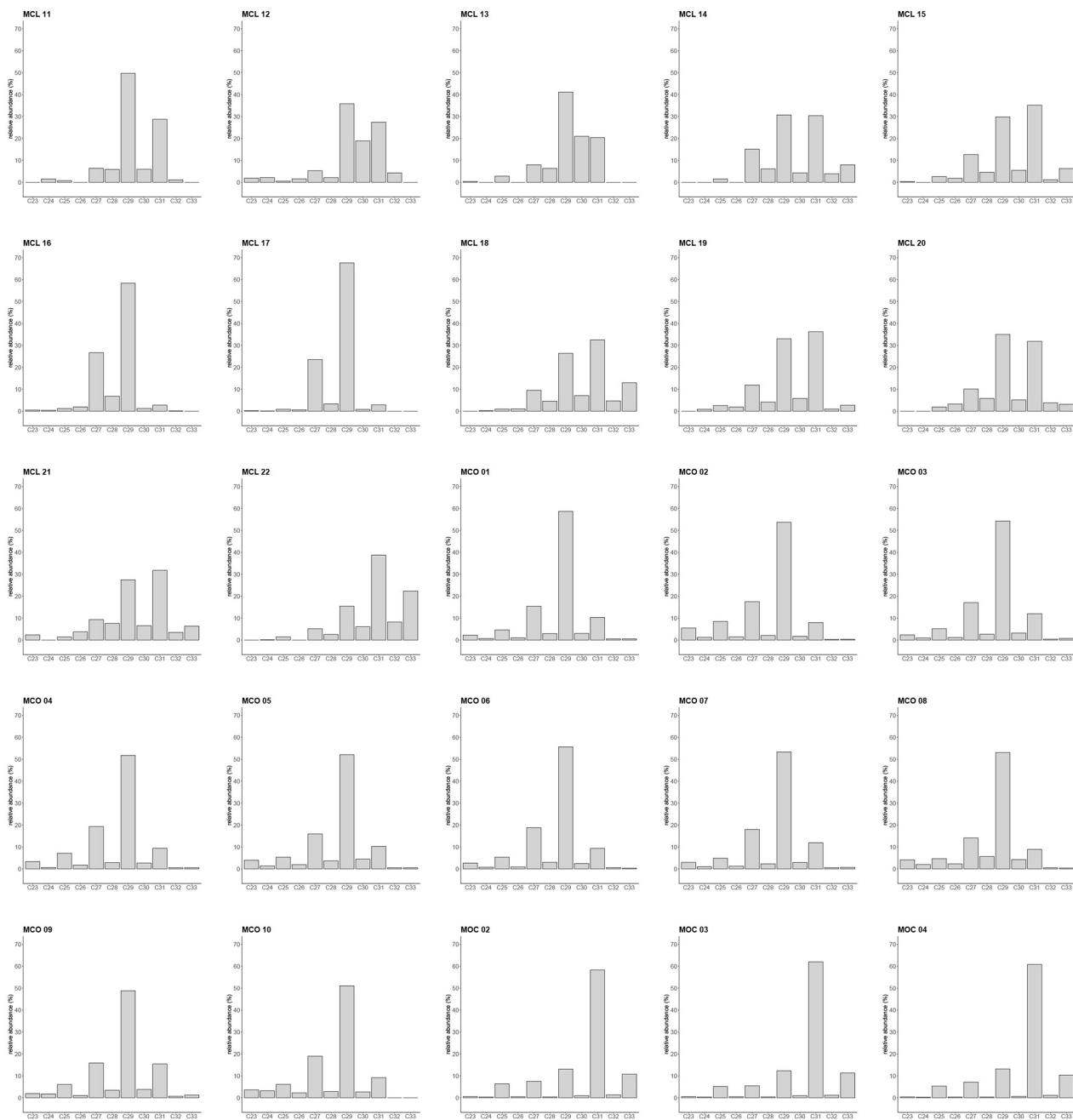
410 **Figure B1 (continued, 6/6)**
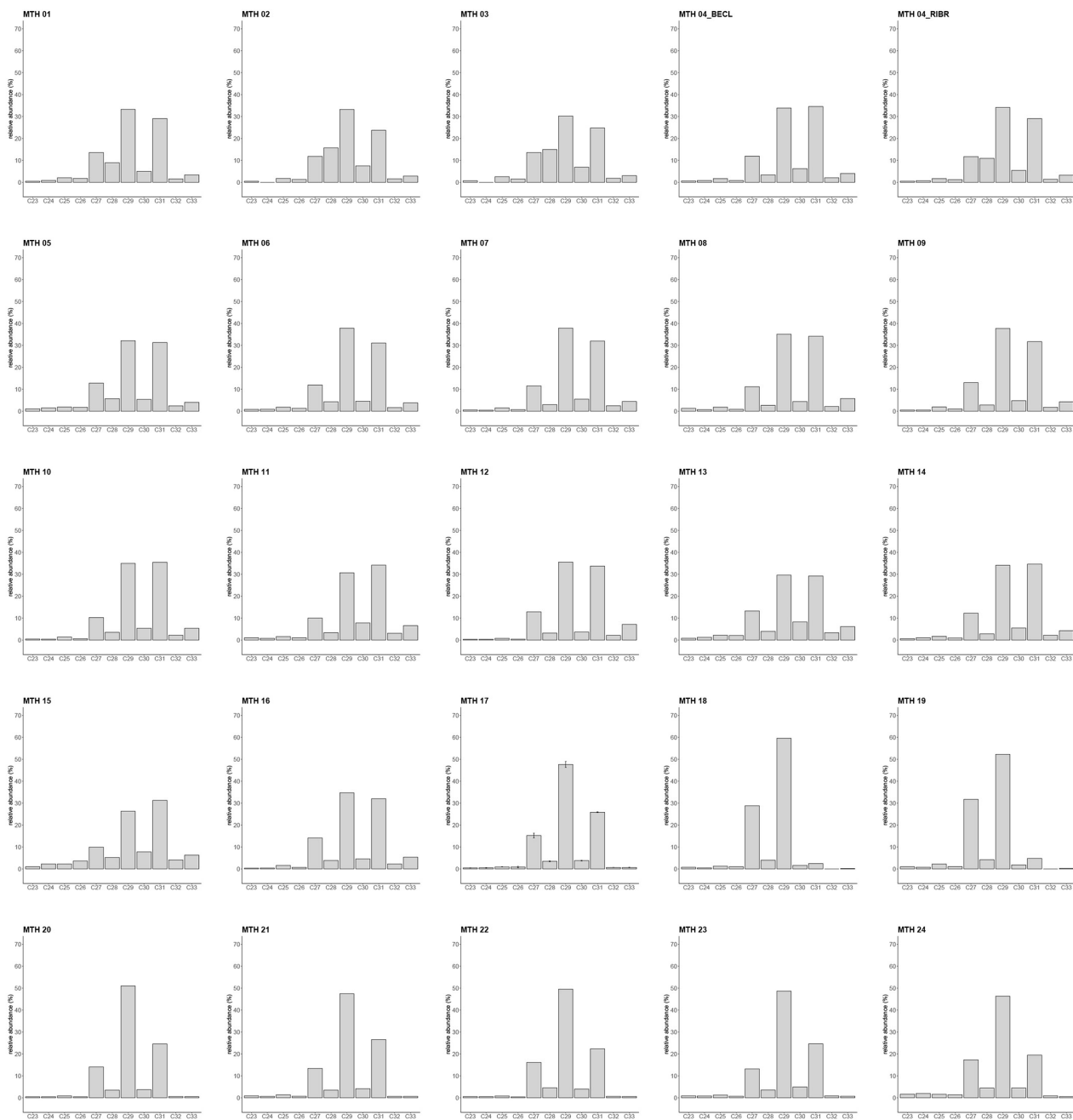
Appendix C

415 **Figure C1: nMDS (a, b) and correlation results (c, d) of the leaf samples without the *Miconia bracteolata* species samples (4 samples in total).**
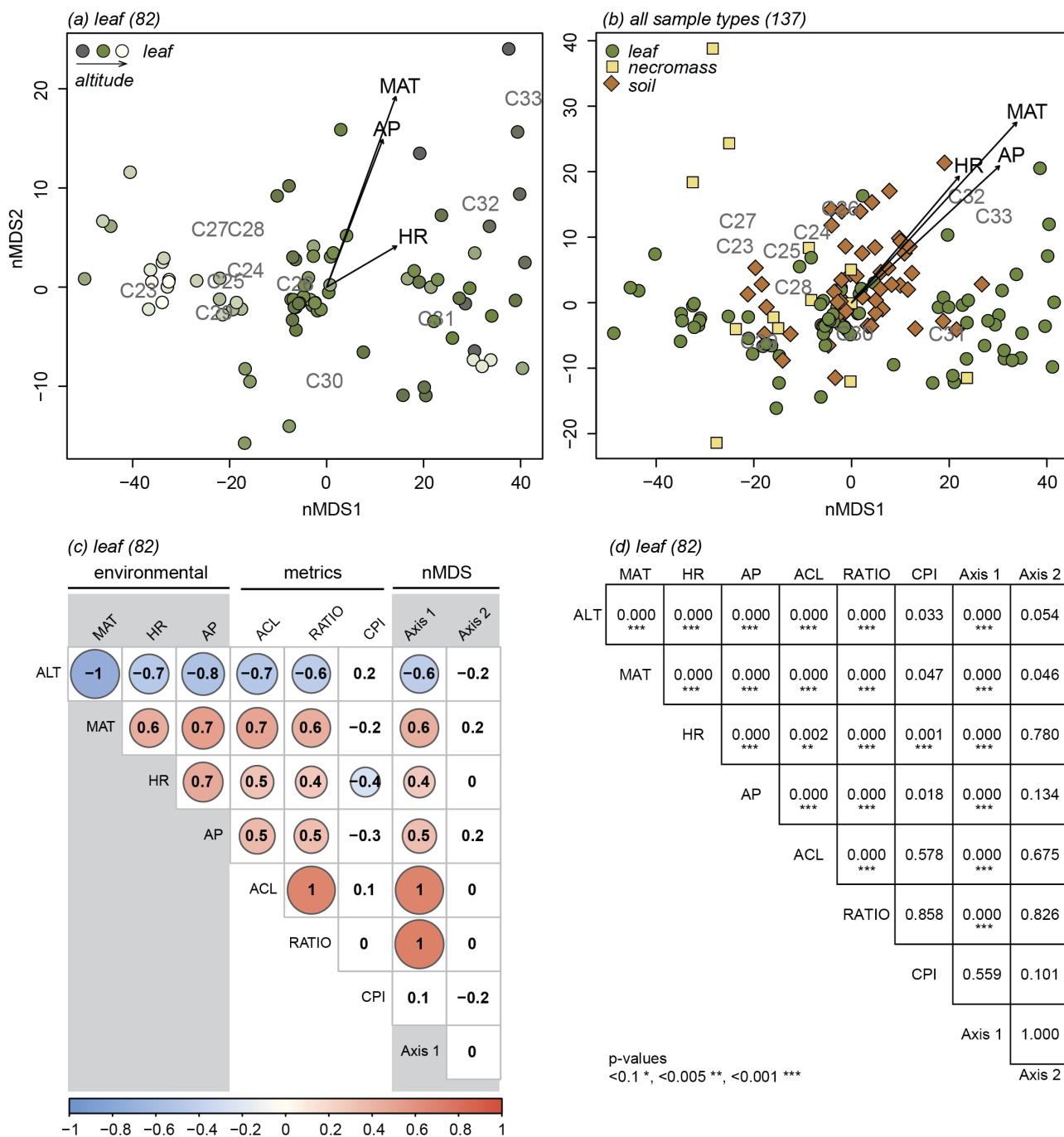
Author contribution

MTVM, WDG and BJ conceived and designed the study. MTVM, FCC and SLY facilitated and conducted fieldwork. MTVM did the lab analysis and analysed the data. MTVM, WDG and BJ wrote the manuscript. All authors contributed to the drafts of the manuscript and its final approval.

Funding

Financial support came the Institute for Biodiversity and Ecosystem Dynamics (University of Amsterdam). Additional funding came from the EcoAndes Project conducted by Consortium for the Sustainable Development of the Andean Ecoregion (CONDESAN) and United Nations Environment Programme (UNEP), funded by the Global Environmental Fund (GEF), cooperation agreement N° 4750.

References

Ardenghi, N., Mulch, A., Pross, J. and Maria Niedermeyer, E.: Leaf wax n-alkane extraction: An optimised procedure, Org. Geochem., 113, 283–292, doi:10.1016/j.orggeochem.2017.08.012, 2017.

Brittingham, A., Hren, M. T. and Hartman, G.: Microbial alteration of the hydrogen and carbon isotopic composition of n-alkanes in sediments, Org. Geochem., 107, 1–8, doi:10.1016/j.orggeochem.2017.01.010, 2017.

Buggle, B., Wiesenberg, G. L. B. and Glaser, B.: Is there a possibility to correct fossil n-alkane data for postsedimentary alteration effects?, Appl. Geochemistry, 25(7), 947–957, doi:10.1016/j.apgeochem.2010.04.003, 2010.

Bush, R. T. and McInerney, F. A.: Leaf wax n-alkane distributions in and across modern plants: Implications for paleoecology and chemotaxonomy, Geochim. Cosmochim. Acta, 117, 161–179, doi:10.1016/j.gca.2013.04.016, 2013.

Bush, R. T. and McInerney, F. A.: Influence of temperature and C4 abundance on n-alkane chain length distributions across the central USA, Org. Geochem., 79, 65–73, 2015.

Carr, A. S., Boom, A., Grimes, H. L., Chase, B. M., Meadows, M. E. and Harris, A.: Leaf wax n-alkane distributions in arid zone South African flora: Environmental controls, chemotaxonomy and palaeoecological implications, Org. Geochem., 67, 72–84, doi:10.1016/j.orggeochem.2013.12.004, 2014.

Crausbay, S., Genderjahn, S., Hotchkiss, S., Sachse, D., Kahmen, A. and Arndt, S. K.: Vegetation Dynamics at the Upper Reaches of a Tropical Montane Forest are Driven by Disturbance Over the Past 7300 Years, Arctic, Antarct. Alp. Res., 46(4), 787–799, doi:10.1657/1938-4246-46.4.787, 2014.

Cronin, T. M.: Paleoclimates, in Global Environmental Change. Handbook of Global Environmental Pollution, vol 1, edited by B. Freedman, pp. 49–54, Springer, Dordrecht, The Netherlands., 2014.

Eglinton, G. and Hamilton, R. J.: Leaf Epicuticular Waxes, Science, 156(3780), 1322–1335, doi:10.1126/science.156.3780.1322, 1967.

Eglinton, T. I. and Eglinton, G.: Molecular proxies for paleoclimatology, Earth Planet. Sci. Lett., 275(1–2), 1–16, doi:10.1016/j.epsl.2008.07.012, 2008.

Feakins, S. J., Peters, T., Wu, M. S., Shenkin, A., Salinas, N., Girardin, C. A. J., Bentley, L. P., Blonder, B., Enquist, B. J.,
450   Martin, R. E., Asner, G. P. and Malhi, Y.: Production of leaf wax n-alkanes across a tropical forest elevation transect, Org. Geochem., 100, 89–100, doi:10.1016/j.orggeochem.2016.07.004, 2016.

Feakins, S. J., Wu, M. S., Ponton, C., Galy, V. and West, A. J.: Dual isotope evidence for sedimentary integration of plant wax biomarkers across an Andes-Amazon elevation transect, Geochim. Cosmochim. Acta, 242, 64–81, doi:10.1016/j.gca.2018.09.007, 2018.

455   Harrell, F. E. and Dupont, C.: Hmisc: Harrell Miscellaneous. R package (version 4.2-0), [online] Available from: https://cran.r-project.org/package=Hmisc, 2019.

Hoffmann, B., Kahmen, A., Cernusak, L. A., Arndt, S. K. and Sachse, D.: Abundance and distribution of leaf wax n-alkanes in leaves of acacia and eucalyptus trees along a strong humidity gradient in Northern Australia, Org. Geochem., 62, 62–67, doi:10.1016/j.orggeochem.2013.07.003, 2013.

460   Howard, S., McInerney, F. A., Caddy-Retalic, S., Hall, P. A. and Andrae, J. W.: Modelling leaf wax n-alkane inputs to soils along a latitudinal transect across Australia, Org. Geochem., 121, 126–137, doi:10.1016/j.orggeochem.2018.03.013, 2018.

Jansen, B. and Wiesenberg, G. L. B.: Opportunities and limitations related to the application of plant-derived lipid molecular proxies in soil science, SOIL, 3, 211–234, doi:10.5194/soil-3-211-2017, 2017.

Jansen, B., de Boer, E. J., Cleef, A. M., Hooghiemstra, H., Moscol-Olivera, M., Tonneijck, F. H. and Verstraten, J. M.:
465   Reconstruction of late Holocene forest dynamics in northern Ecuador from biomarkers and pollen in soil cores, Palaeogeogr. Palaeoclimatol. Palaeoecol., 386, 607–619, doi:10.1016/j.palaeo.2013.06.027, 2013.

Karger, D. N., Conrad, O., Böhner, J., Kawohl, T., Kreft, H., Soria-Auza, R. W., Zimmermann, N. E., Linder, H. P. and Kessler, M.: Climatologies at high resolution for the earth's land surface areas, Sci. Data, 4, 1–20, doi:10.1038/sdata.2017.122, 2017.

470   Luo, P., Peng, P. A., Lü, H. Y., Zheng, Z. and Wang, X.: Latitudinal variations of CPI values of long-chain n-alkanes in surface soils: Evidence for CPI as a proxy of aridity, Sci. China Earth Sci., 55(7), 1134–1146, doi:10.1007/s11430-012-4401-8, 2012.

Marzi, R., Torkelson, B. E. and Olson, R. K.: A revised carbon preference index, Org. Geochem., 20(8), 1303–1306, doi:10.1016/0146-6380(93)90016-5, 1993.

475   Oksanen, J., Blanchet, F. G., Friendly, M., Kindt, R., Legendre, P., McGlinn, D., Minchin, P. R., O'Hara, R. B., Simpson, G. L., Solymos, P., Stevens, M. H. H., Szoecs, E. and Wagner, H.: vegan: Community Ecology Package. R package version 2.5-5., , https://cran.r-project.org/package=vegan, doi:https://CRAN.R-project.org/package=vegan, 2018.

Pinto, E. and Cuesta, F.: Monitoreo de Biodiversidad, Contenidos de Carbono, Productividad y Rasgos funcionales en Bosques Montanos, CONDESAN, Quito, Ecuador., 2019.

480   Pinto, E., Pérez, Á. J., Ulloa Ulloa, C. and Cuesta, F.: Arboles representativos de los bosques montanos del noroccidente de

Pichincha, Ecuador, CONDESAN, Quito, Ecuador., 2018.

R Core Team: R: A language and environment for statistical computing., , https://www.r-project.org/ [online] Available from: https://www.r-project.org/, 2017.

Rao, Z., Zhu, Z., Wang, S., Jia, G., Qiang, M. and Wu, Y.: CPI values of terrestrial higher plant-derived long-chain n-alkanes: A potential paleoclimatic proxy, Front. Earth Sci. China, 3(3), 266–272, doi:10.1007/s11707-009-0037-1, 2009.

Smol, J. P., Birks, H. J. B. and Last, W. M., Eds.: Tracking Environmental Change Using Lake Sediments. Volume 3: Terrestrial, Algal, and Siliceous Indicators., Springer, Dordrecht, The Netherlands., 2001.

Teunissen van Manen, M. L., Jansen, B., Cuesta, F., León-Yánez, S. and Gosling, W. D.: Leaf wax n-alkane patterns of six tropical montane tree species show species-specific environmental response, Ecol. Evol., 9(9), 9120–9128, doi:10.1002/ece3.5458, 2019.

Tipple, B. J. and Pagani, M.: Environmental control on eastern broadleaf forest species' leaf wax distributions and d/h ratios, Geochim. Cosmochim. Acta, 111, 64–77, doi:10.1016/j.gca.2012.10.042, 2013.

Wang, J., Xu, Y., Zhou, L., Shi, M., Axia, E., Jia, Y., Chen, Z., Li, J. and Wang, G.: Disentangling temperature effects on leaf wax n-alkane traits and carbon isotopic composition from phylogeny and precipitation, Org. Geochem., 126, 13–22, doi:10.1016/j.orggeochem.2018.10.008, 2018.

Wei, T. and Simko, V.: R package "corrplot": visualization of a correlation matrix (version 0.84), [online] Available from: https://github.com/taiyun/corrplot, 2017.

Wickham, H.: tidyverse: Easily Install and Load the "Tidyverse" (version 1.2.1), [online] Available from: https://cran.r-project.org/package=tidyverse, 2017.

Wu, M. S., West, A. J. and Feakins, S. J.: Tropical soil profiles reveal the fate of plant wax biomarkers during soil storage, Org. Geochem., 128, 1–15, doi:10.1016/j.orggeochem.2018.12.011, 2019.

505 **Table 1: Sampling table. Plot numbers refer to numbers in Figure 1. Plot codes refer to specific plots within the natural reserve, situated at their respective longitude and latitude. Altitude, temperature (MAT), humidity (HR) and precipitation (AP) data corresponding to each plot is included. Table notes what sample types were taken (sample type), how many were taken (sampled) and which samples were measured successfully and included in analysis (n).**

plot #	plot code	reserve	latitude	longitude	altitude	MAT	HR	AP	sample type	sampled	n
1	MAPI_02	Mashpishungo/Pambiliño	0.1882	-78.9128	632	21.6	99.8	2111	soil	3	3
2	MAPI_01	Mashpishungo/Pambiliño	0.1873	-78.9128	653	21.6	99.8	2075	leaf	2	2
									necro	5	3
									soil	3	3
3	MALO_01	Mashpi Lodge	0.1583	-78.8819	827	19.4	99.6	2255	leaf	3	3
									soil	4	4
4	MALO_02	Mashpi Lodge	0.1685	-78.8761	1018	20.6	99.7	2253	leaf	3	3
									soil	3	3
5	MIND_01	Mindo Lindo	-0.0253	-78.8129	1277	18.8	98.9	2704	leaf	4	4
									soil	3	3
6	RIBR_01	Reserva Rio Bravo	-0.082	-78.7353	1640	16.8	98.8	2347	leaf	12	12
									soil	3	3
7	INTI_02	Reserva Intillacta	0.0501	-78.7219	1829	15.9	99.0	1939	soil	3	3
8	INTI_01	Reserva Intillacta	0.0505	-78.7232	1879	16.0	98.8	2076	leaf	1	1
									necro	5	5
									soil	3	3
9	BECL_03	Bellavista Cloud Forest	-0.0116	-78.6893	2203	14.0	99.6	1595	leaf	8	8
									soil	3	3
10	CEDR_03	El Cedral Ecolodge	0.1132	-78.5691	2212	14.3	98.6	1351	leaf	11	11
									necro	5	5
									soil	3	2
11	BECL_02	Bellavista Cloud Forest	-0.0124	-78.6864	2282	14.3	99.1	1993	soil	3	3
12	BECL_01	Bellavista Cloud Forest	-0.0153	-78.6863	2313	13.6	99.3	1595	leaf	8	8
									soil	3	3
13	CEDR_01	El Cedral Ecolodge	0.1195	-78.5705	2492	13.0	97.7	1471	leaf	9	9
									soil	3	3
14	VERD_02	Reserva Verdecocha	-0.1015	-78.6004	2932	10.2	99	1251	leaf	4	4
									soil	3	3
15	VERD_03	Reserva Verdecocha	-0.1044	-78.6008	3109	9.9	96.2	1251	leaf	6	6
									soil	3	3
16	VERD_01	Reserva Verdecocha	-0.1233	-78.5958	3421	8.3	97	1271	leaf	8	7
									soil	3	3
17	YANA_01	Reserva Yanacocha	-0.1267	-78.5907	3507	7.2	98.7	1337	leaf	8	8
									soil	3	3

510

Table 2: Table containing the p-values of the Pearson's correlation coefficients depicted in Figure 4 and Figure 5. Per sample type (a,b,c), the correlated variables are: Altitude (ALT), temperature (MAT), humidity (HR), average chain length (ACL), ratio $C_{31}/(C_{31}+C_{29})$ (RATIO), carbon preference index (CPI), and the two axis of the nMDS analysis of each sample type (Axis 1, Axis 2).

	MAT	HR	AP	ACL	RATIO	CPI	Axis 1	Axis 2
ALT	0.000 ***	0.000 ***	0.000 ***	0.000 ***	0.000 ***	0.100	0.000 ***	0.506
	MAT	0.000 ***	0.000 ***	0.000 ***	0.000 ***	0.145	0.000 ***	0.391
		HR	0.000 ***	0.002 **	0.000 ***	0.001 **	0.000 ***	0.107
			AP	0.000 ***	0.000 ***	0.035	0.000 ***	0.907
				ACL	0.000 ***	0.272	0.000 ***	0.001 **
a) *leaf (86)*					RATIO	0.611	0.000 ***	0.531
						CPI	0.389	0.005 **
							Axis 1	1.000
								Axis 2

	MAT	HR	AP	ACL	RATIO	CPI	Axis 1	Axis 2
ALT	0.000 ***	0.000 ***	0.000 ***	0.317	0.757	0.211	0.191	0.276
	MAT	0.000 ***	0.000 ***	0.304	0.764	0.222	0.186	0.256
		HR	0.000 ***	0.328	0.752	0.203	0.197	0.295
			AP	0.157	0.923	0.591	0.141	0.051
				ACL	0.001 ***	0.588	0.000 ***	1.000
b) *necromass (13)*					RATIO	0.226	0.000 ***	0.058
						CPI	0.426	0.224
							Axis 1	1.000
								Axis 2

	MAT	HR	AP	ACL	RATIO	CPI	Axis 1	Axis 2
ALT	0.000 ***	0.000 ***	0.000 ***	0.000 ***	0.001 **	0.004 **	0.000 ***	0.897
	MAT	0.000 ***	0.000 ***	0.000 ***	0.001 ***	0.005 **	0.000 ***	0.792
		HR	0.000 ***	0.171	0.348	0.030	0.163	0.416
			AP	0.001 **	0.017	0.005	0.005 **	0.843
				ACL	0.000 ***	0.907	0.000 ***	0.164
c) *soil (51)*					RATIO	0.420	0.000 ***	0.513
						CPI	0.291	0.001 ***
p-values							Axis 1	1.000
<.01 *, <0.005 **, <0.001 ***								Axis 2

Figure 1: Map of the Pichincha transect. Dots and numbers refer to plots in Table 1, ordered by altitude. The green shading indicates altitude (m above sea level). The black line delineates the Pichincha project study area. Blue lines represent rivers, land codes as follows: COL = Colombia, ECU = Ecuador, PER = Perú.
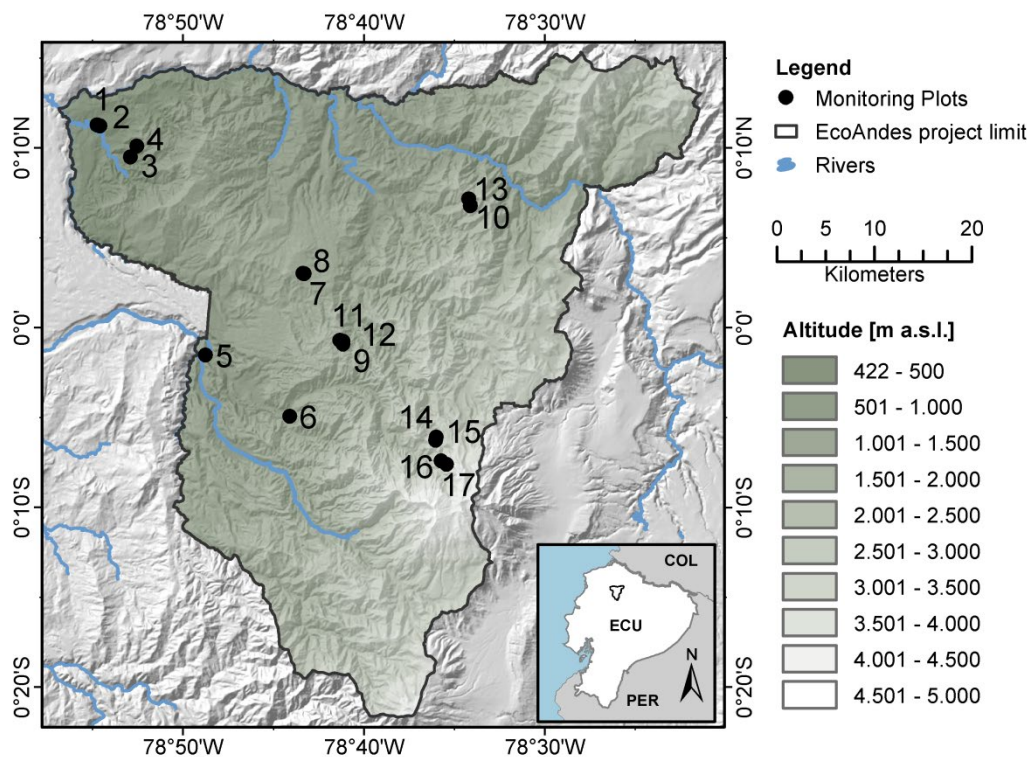
520

Figure 2: Sample type average *n*-alkane distributions along the transect, showing average relative abundances (average % of total concentration (CONw)) across entire transect. Lines represent standard deviation from average, numbers in parentheses represent number of samples.

525
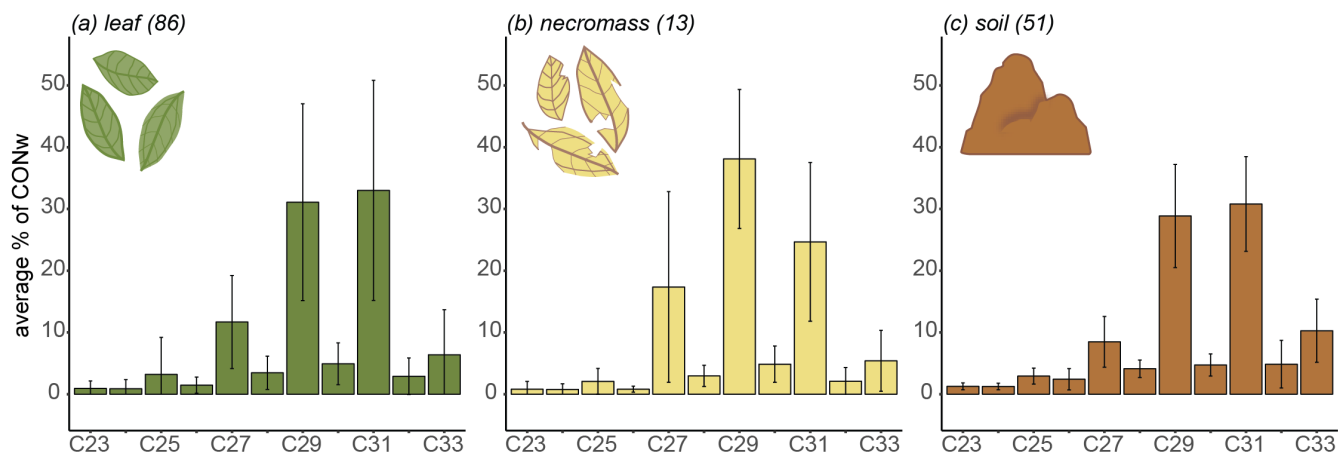
Figure 3: nMDS plots of *n*-alkane patterns per sample type (a,b,c) and all sample types combined (d). Numbers in parentheses next to sample type represent number of samples. Arrows indicate fit of environmental variables, altitude (ALT), temperature (MAT), humidity (HR) and precipitation (AP). Text indicate *n*-alkane chain length contribution to sample. Samples indicated by symbols, sample type indicated by symbol color and shape (green circles = leaf, yellow squares = necromass, brown diamonds = soil). Colour gradient in panels a, b and c indicate altitude (darker = lower, lighter = higher).

530
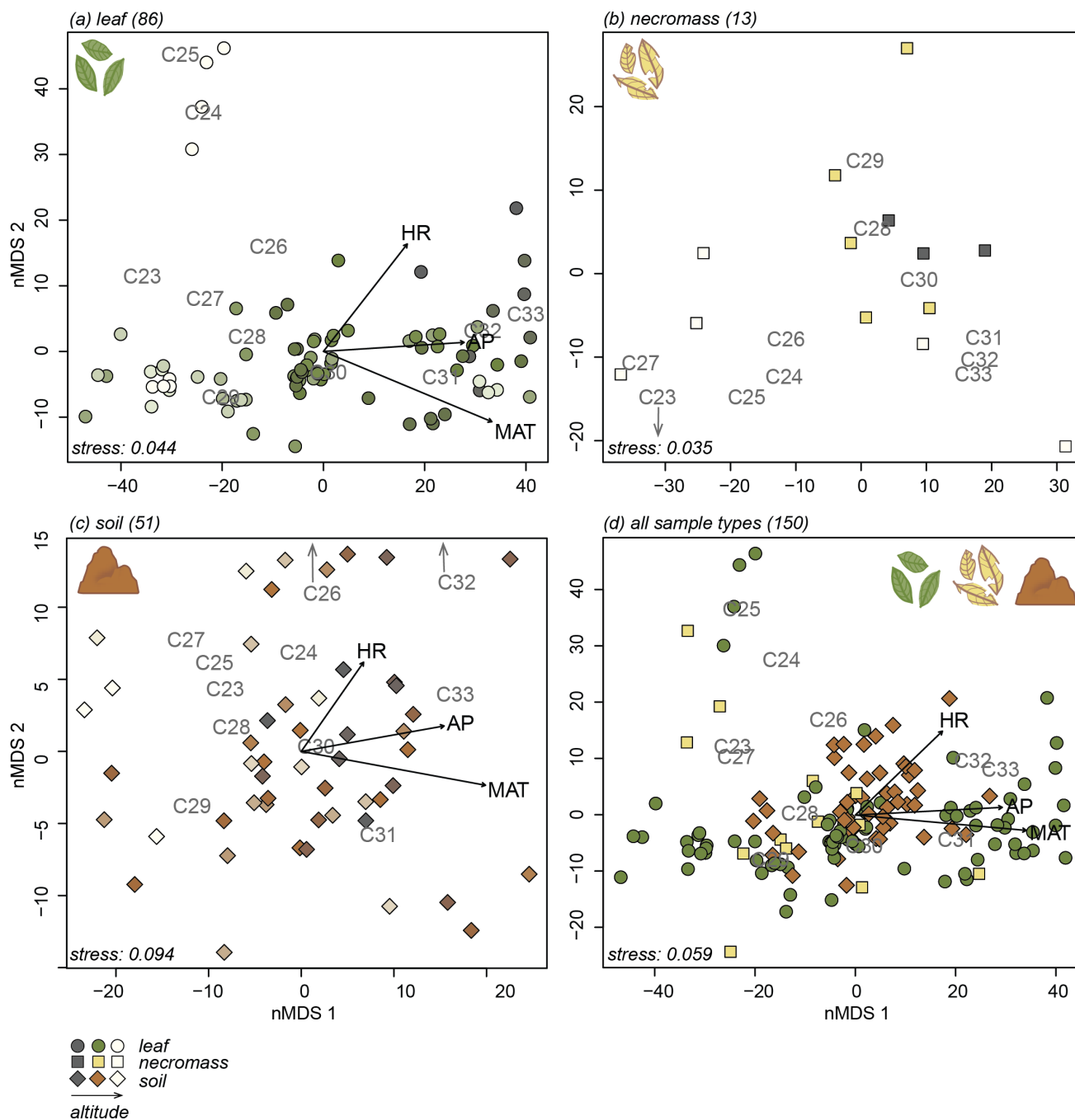
Figure 4: Pearson's correlation coefficient matrix per sample type (a,b,c) showing the correlations between environmental variables (ALT = altitude, MAT = temperature, HR = humidity, AP = precipitation), *n*-alkane metrics (ACL = average chain length, RATIO = ratio $C_{31}/(C_{31}+C_{29})$, CPI = carbon preference index) and the nMDS axes (Axis 1, Axis 2). Numbers in parentheses represent number of samples. Significant correlations are circled, where the color and circle size indicate the direction and correlation strength. Circle outlines reflect the significance level. Non-significant correlations are not circled.

545 **Figure 5: Scatterplots of *n*-alkane metrics (ACL = average chain length, RATIO = $C_{31}/(C_{31}+C_{29})$, CPI = carbon preference index) along the environmental gradient (MAT = temperature, HR = humidity, AP = precipitation). Symbols and colors indicate sample type (green circles = leaf, yellow squares = necromass, brown diamonds = soil), numbers in parentheses represent number of samples. Shading indicates the standard error of the linear correlation (lines), line type represents the significance level of the correlation. Represented correlation coefficients and p-values correspond to values in Figure 4 and Table 2.**